Hindawi
International Journal of Antennas and Propagation
Volume 2021, Article ID 1559519, 7 pages
https://doi.org/10.1155/2021/1559519

Research Article

A Novel "回" Pattern Branch Antenna for 3G\4G\WLAN\Bluetooth\Navigation Applications

Tangyao Xie,[1] **Jianguo Yu**,[1] **Yao Li**,[2] **Zhen Yu**,[2] **and Ziheng Lin**[2]

[1]*Beijing Key Laboratory of Work Safety Intelligent Monitoring (Beijing University of Posts and Telecommunications), Beijing, China*
[2]*North China Institute of Science and Technology, Langfang, China*

Correspondence should be addressed to Zhen Yu; yzyuzhen@ncist.edu.cn

Received 31 August 2021; Revised 25 October 2021; Accepted 10 November 2021; Published 24 November 2021

Academic Editor: Chien-Jen Wang

This study proposes and designs a multiband branch antenna with a structure that imitates the Chinese classical pattern structure. The antenna radiator's structure is a symmetrical rectangular stub fused with a Chinese classical pattern structure, and the rectangular stub is bent so that the outer and inner stubs are coupled to each other to generate multiple frequency bands. Microstrip line feeding is the feeding mode, and the grounding plate is a trapezoidal structure formed by subtracting two triangles from a rectangle. The overall size of the antenna is $60 \times 60 \times 1.6\ mm^3$, and the dielectric board adopts FR4. The substrate dielectric constant $\varepsilon r = 4.4$, the thickness $h = 1.6$ mm, and the dielectric loss tangent $\tan\delta = 0.02$. For antenna modeling and parameter optimization, HFSS electromagnetic simulation software is used. The antenna can cover 1.49 to 1.60 GHz, 1.87 to 2.51 GHz, and 4.63 to 5.34 GHz and generate three main frequencies: 1.57, 2.15, and 5.06 GHz, according to test result. The antenna has omnidirectional radiation characteristics and can be widely used in future mobile communication network coverage.

1. Introduction

Since the invention of the antenna, the antenna has played an increasingly important role in human social life. It is a vital radio device for transmitting and receiving electromagnetic waves, as well as an essential component of the radio communication system. The performance of the antenna has a direct impact on the communication system's quality. Modern communications have paid increasing attention to the study of antenna multiband miniaturization performance to improve the efficiency and performance of antennas [1, 2].

Imitating the classical grille structure multiband antenna and combining the unique structure of the classic grille with the theory of antenna design, the changeable pattern inside the grille can make the antenna have multiband performance characteristics. By changing the structure of the window grille, the influence of its structure on the antenna performance is analyzed, and the structure that makes the antenna performance the best is found [3].

The door and window patterns that can be used for antenna design are broadly classified as geometric patterns, tree and flower patterns, animal patterns, and so on. Geometric patterns are those that use straight lines, curves, and shapes to create geometric patterns for decorations. It can be combined in many ways, including ice crack, step-by-step brocade, swastika pattern, set of square brocade, "回" pattern [4], and so on. In this antenna design, the structure of the "回" pattern is adopted, as shown in Figure 1.

Multifrequency band technology is to increase the path through which current flows on the surface of the radiator to generate resonance and realize multifrequency bands. Multipatch technology, slot-loading technology, multibranch structure, fractal structure, and other multiband implementation technologies are currently in use. By incorporating one or more patches, the radiator can operate in various resonant modes, generating multiple resonant frequency points to form a multiband antenna [5, 6]. Open one or more slots on the surface of the radiator to extend the path of the antenna surface current, change the path of the surface

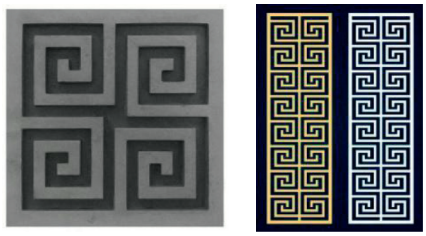

Figure 1: "回" word pattern structure.

current, and make the multiple resonance frequencies which are generated by the radiator [7–9]. The antenna extends the radiator's branches and uses electromagnetic coupling to generate multiple frequency points [10–12]. Using the self-similarity of the fractal structure, after a certain number of iterations, each part of the radiator corresponds to a different resonance frequency to achieve the multiband performance of the antenna [13]. Taha A. Elwi et al. proposed a metamaterial (MTM) antenna series. It combines INP substrate and fractal technology. Part of the structure is similar to the "回" pattern structure, but the performance of the two differs due to differences in substrate material power supply mode [14].

In this paper, using the technique of multiple branches, combined with the classical pattern window grille structure, a design of a "回" pattern branch antenna with multiband characteristics is proposed and discussed. In the window grille structure, the "回" pattern is a relatively simple geometric pattern. The surface current path and length of the antenna are increased by bending the rectangular radiator into multiple branches, resulting in multiband performance. The antenna was designed to cover three frequency bands: 1.49–1.60 GHz, 1.87–2.51 GHz, and 4.63–5.34 GHz. It has a wide range of applications, including GPS, Beidou navigation systems, 3G, 4G, WLAN, Bluetooth, WIMAX, and other communication systems.

2. Design and Structure of Antenna

The electromagnetic simulation software HFSS is used to optimize the antenna parameters. Figure 2 depicts the final antenna structure model. Table 1 displays the size parameters. The dielectric plate is made of polytetrafluoroethylene glass cloth (FR4) with a dielectric constant $\varepsilon_r = 4.4$, a thickness of 1.6 mm, and a dielectric loss tangent tan of $\delta = 0.02$. The physical size of the media board is $60 \times 60 \times 1.6\ \text{mm}^3$.

3. Parameter Optimization

The main shape of the antenna is a rectangular stub, which incorporates a "回" pattern structure. The rectangular stub is bent into a "回" pattern structure, and a microstrip line structure is used for power feeding, bending the radiator and the electromagnetic coupling effect is primarily responsible for the multifrequency performance. Figure 3 depicts the evolution of the antenna.

In Figure 3, model (a) is a basic antenna model. The antenna model mimics the structure of the "回" pattern, by

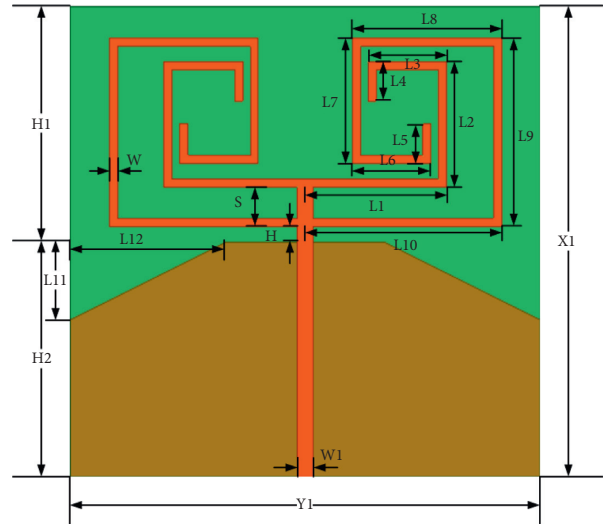

Figure 2: Antenna model size drawing.

Table 1: Antenna parameters.

Parameter	X1	Y1	H	H1	H2	W	W1
Value (mm)	60	60	2	30	30	1	2
Parameter	S	L1	L2	L3	L4	L5	L6
Value (mm)	5	18	15	9	4	4	9
Parameter	L7	L8	L9	L10	L11	L12	
Value (mm)	15	18	23	25	10	20	

bending the rectangular branches to form two inner and outer loops, with a fixed distance between each inner and outer branch. During the optimization of stimulation parameters, it was discovered that only two frequency points, 2.8 GHz and 5.8 GHz, have the antenna's return loss value less than −10 dB. On this basis, the grounding plate was changed, and the two right angles above the grounding plate were cut off, and the structure is shown in model (b) appeared. Model (b) has three more frequency points than model (a), 2.4 GHz, 3.8 GHz, and 5.1 GHz, and generates five usable frequency bands. Based on model (b), model (c) cancels the fixed distance between the inner and outer branches, resulting in each branch having its own parameter value. After a series of parameter optimization, the structure is shown in model (c) appears. The return loss diagram of the three evolution process is shown in Figure 3.

By comparing and analyzing the comparison chart of return loss curve in Figure 4, model (c) produced six resonance frequency points of 1.55 GHz, 2.4 GHz, 3.11 GHz, 4.1 GHz, 5.05 GHz, and 5.84 GHz, resulting in six frequency band: 1.49–1.58 GHz, 1.81–2.55 GHz, 2.74–3.42 GHz, 3.68–4.29 GHz, 4.72–5.38 GHz, and 5.59–6.12 GHz. At 2.4 GHz, the −10 dB bandwidth of model antenna (c) is 0.3 GHz narrower than that of model (b), and at 3.11 GHz, the −10 dB bandwidth of model antenna (c) is 0.4 GHz wider than model (b), and the return loss value is low. The return loss and bandwidth of the antenna do not change significantly in the high-frequency region. Comprehensive comparison, the model antenna (c) has superior performance in all aspects, so it is chosen as the final antenna model.

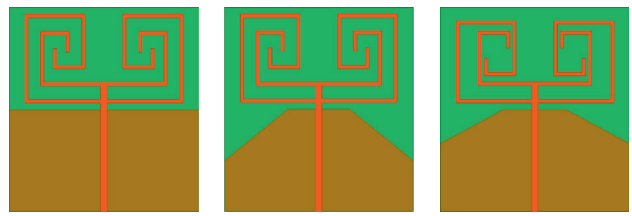

Figure 3: The evolution of antennas.

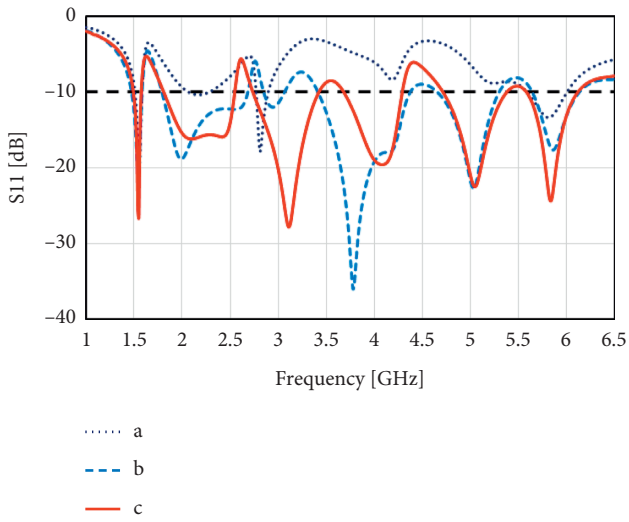

Figure 4: Comparison chart of return loss during antenna evolution.

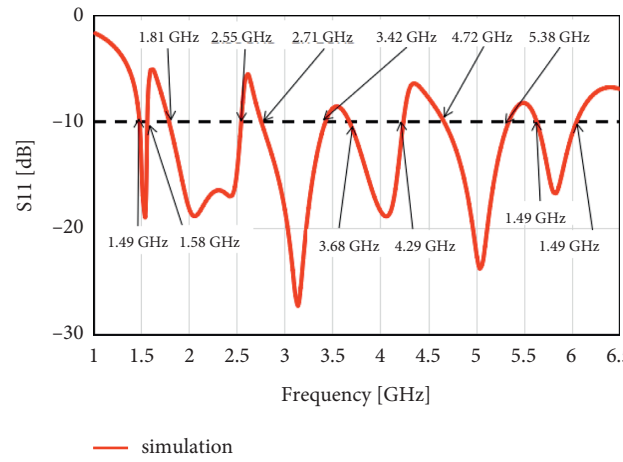

Figure 5: Antenna's return loss graph.

4. Antenna Simulation Results and Parameter Analysis

Figure 5 shows the return loss curve of the antenna. The antenna has six different resonant frequency bands. The center frequency points are 1.55 GHz, 2.4 GHz, 3.11 GHz, 4.1 GHz, 5.05 GHz, and 5.84 GHz, and the return loss values at the six resonance frequency points are −26.59 dBi, −15.89 dBi, −27.84 dBi, −19.56 dBi, −22.52 dBi, and −24.37 dBi. According to the return loss ≤−10 dB as the reference standard, from the return loss diagram, the −10 dB bandwidth corresponding to the center resonance frequency point on the return loss diagram is 1.49–1.58 GHz, 1.81–2.55 GHz, 2.74–3.42 GHz, 3.68–4.29 GHz, 4.72–5.38 GHz, and 5.59–6.12 GHz. Table 2 shows the the communication frequency bands covered by these frequency bands.

Figure 6 is the surface current and vector distribution diagram of the antenna at the resonance frequencies of 1.55 GHz, 2.4 GHz, 3.11 GHz, 4.1 GHz, 5.05 GHz, and 5.84 GHz.

It can be seen from the surface current distribution of the antenna in Figure 6. When the center frequency is 1.55 GHz, the antenna surface current is primarily focused at the end of the radiator branch, the current is relatively smooth, and the impedance is matched. At 2.4 GHz, the current path becomes shorter as the frequency increases, and the current is primarily concentrated on the bottom of the radiator and the feeder. At the frequency point of 5.05 GHz, the surface current of the antenna is mainly concentrated on the radiator and the feeder, and the branches of the radiator are electromagnetically coupled with the ground plate so that the current spreads across the branches of the radiator. The antenna current is primarily concentrated on the feeder at the frequency point of 5.84 GHz. The antenna generates resonance frequency points primarily by changing the electromagnetic coupling between the current direction and the feeder stubs. A lower frequency corresponds to a longer current path, while a higher frequency corresponds to a shorter current path.

Table 2: Antenna's commercial communication frequency band.

Frequency band	Communication frequency band
1.49–1.58 GHz (6%)	GPS (1.575–1.625 GHz)
	Bluetooth (2.4–2.485 GHz)
	WLAN (2.4–2.4835 GHz)
1.81–2.55 GHz (31%)	LTE Band40 (2.3–2.4 GHz)
	ISM Band (2.420–2.4835 GHz)
	WiMAX (2.3 GHz)
4.72–5.38 GHz (13%)	WLAN (802.11a/*n*:5.15–5.35 GHz)
5.59–6.12 GHz (9%)	5G (5.725–5.825 GHz)

Figures 7(a)–7(d), respectively, list the 3D pattern and the *E* and H plane patterns of the antenna at different central frequencies. The red solid line represents the *E* plane pattern, while the blue dashed line represents the *H* surface direction map. Maximum gains are 1.74 dBi, 3.14 dBi, 2.90 dBi, and

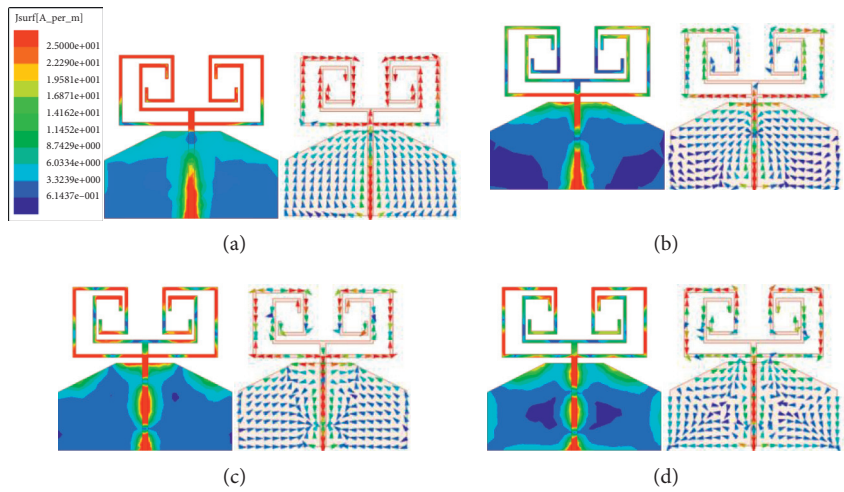

Figure 6: Surface current and vector diagram: (a) 1.55 GHz, (b) 2.4 GHz, (c) 5.05 GHz, and (d) 5.84 GHz.

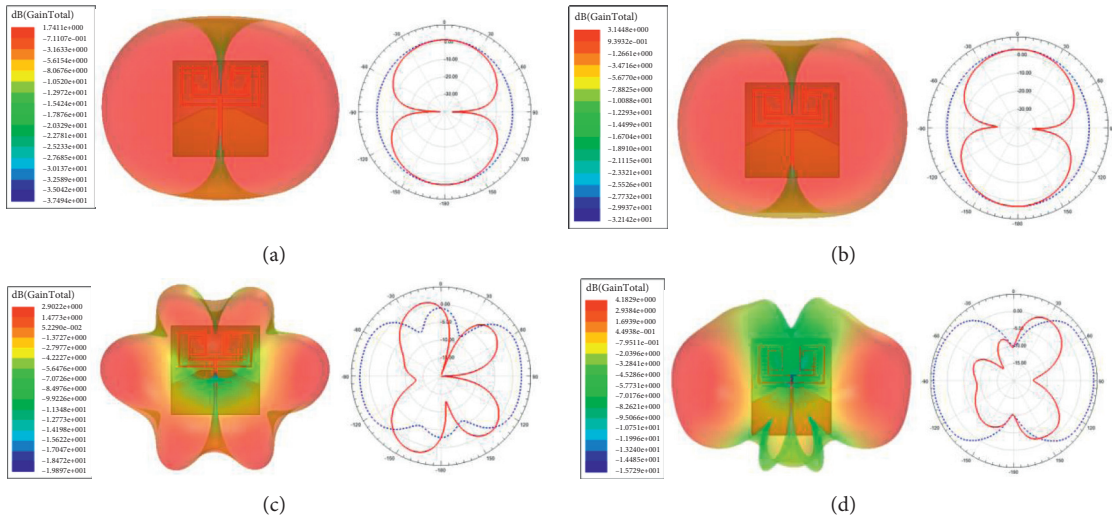

Figure 7: 3D gain radiation pattern and EH surface pattern of the antenna: (a) 1.55 GHz, (b) 2.4 GHz, (c) 5.05 GHz, and (d) 5.84 GHz.

4.18 dBi for antenna center frequencies of 1.55 GHz, 2.4 GHz, 5.05 GHz, and 5.84 GHz, respectively. Overall, the gain of the antenna at each frequency point is sufficient to meet the communication requirements, and the performance is satisfactory. The pattern of the *E* surface changes from a positive figure eight to a concave persimmon shape as frequency increases accompanied by the appearance of side lobes. The *H* surface gradually becomes concave and curved from a circle.

5. Test Results of the Branch Antenna

To verify the correctness of the design, the antenna shown in Figure 8 has been manufactured. The size of the antenna is $60 \times 60 \times 1.6\,\text{mm}^3$. The feeder is connected to a 50 Ω SMA adapter, and the prototype is tested using a vector analyzer and an antenna microwave anechoic chamber.

The comparison between the actual measurement results and the simulation results of the return loss S11 is shown in Figure 9. According to the comparison diagram of the antenna return loss value between the simulation and the actual measurement, it can be seen that the antenna simulation and actual measurement trends are roughly the same.

At the 1.55 GHz frequency point, the frequency point did not move, and the return loss value changed from −18.9 dB to −21.9 dB. The −10 dB bandwidth at 2.4 GHz narrows. The bandwidth is reduced by 0.17 GHz from 1.76–2.56 GHz to 1.87–2.50 GHz. The antenna's resonant frequency is nearly constant at 5.05 GHz; the return loss value has changed from −23.82 dB to −30.78 dB, and the bandwidth is relatively consistent. In the actual measurement, the frequency point of 5.8 GHz is greater than −10 dB. Figure 10 depicts the antenna's actual measured 3D radiation pattern. It can be seen from the actual measured 3D pattern of the antenna that the gain values of the antenna at 1.57, 2.15, and 5.05 GHz are 3.1, 1.76, and 2.54 dBi, respectively. In the low-frequency band, the antenna has better omnidirectional radiation characteristics; as the frequency increases, more side lobe levels and side lobes appear in the 3D radiation

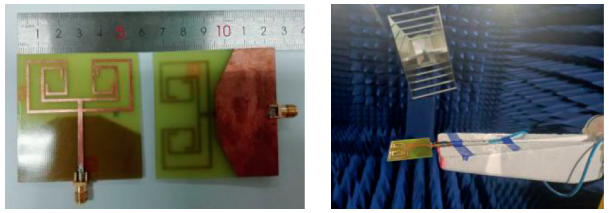

(a) (b)

Figure 8: (a) Antenna physical object. (b) Antenna test.

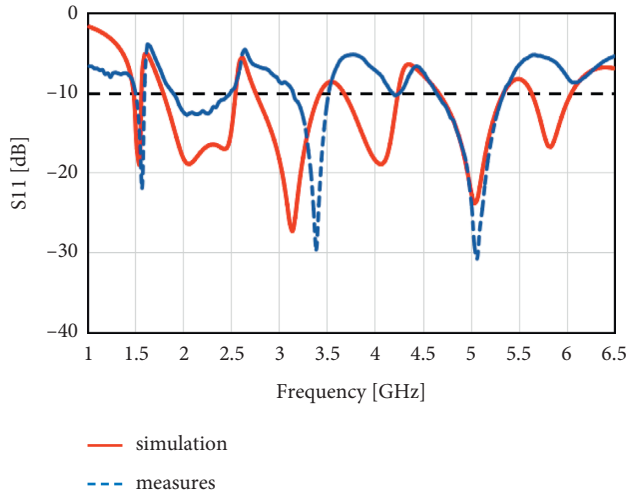

Figure 9: Comparison of simulation and actual measurement of the antenna.

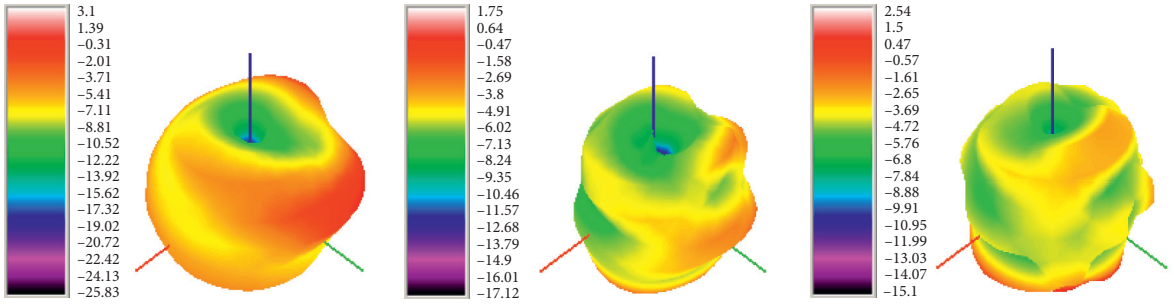

(a) (b) (c)

Figure 10: Measured 3D radiation patterns: (a) 1.57 GHz, (b) 2.15 GHz, and (c) 5.05 GHz.

pattern. The antenna maintains good radiation characteristics throughout its operating frequency range, and there is no zero point. Table 3 shows the specific commercial frequency bands that are available. There is a small difference between the antenna test results and the simulation results due to errors in the artificial manufacturing process of the antenna and electromagnetic interference during the antenna test. On the whole, the actual measurement results of the antenna match the simulation results and meet the design requirements.

Table 3: Antenna's commercial communication frequency band.

Frequency band	Communication frequency band
1.49–1.60 GHz (7%)	GPS L1 (1575.42 ± 1.023 MHz)
	BD 2 (1561.098 ± 2.046 MHz)
1.87–2.51 GHz (29.77%)	TD-SCDMA (1880–2025 MHz) WCDMA (1920–2170 MHz) CDMA2000 (1920–2125 MHz)
	LTE Band40 (2300–2400 MHz)
	ISM Band (2.420–2.4835 GHz)
	WiMAX (2300 MHz)
	Bluetooth (2400–2485 MHz)
	WLAN (802.11 b/g/*n*: 2400–2480 MHz)
	BD1 S (2491.75 ± 4.08 MHz)
4.63–5.34 GHz (14.03%)	WLAN (802.11a/*n*:5150–5350 MHz)

6. Conclusions

Based on the theory of branch antennas, combined with the trapezoidal ground structure, a microstrip branch antenna with multiband characteristics is designed by simulating the classical "回" structure. The comparison of simulation and actual measurement results validates the design's logic. The antenna has a lovely appearance and performs admirably. The antenna dimensions are $60 \times 60 \times 1.6\ \text{mm}^3$. In Figure 10, the central resonance points at 1.57 GHz, 2.15 GHz, and 5.06 GHz reach −21.9 dB, −12.69 dB, and −30.79 dB, respectively, and the maximum gains are 3.1 dBi, 1.75 dBi, and 2.54 dBi, respectively. The pattern branch antenna has three frequency bands, 1.49–1.60 GHz, 1.87–2.51 GHz, and 4.63–5.34 GHz, with relative bandwidths of 7.0%, 29.77%, and 14.03%, respectively, and omnidirectional radiation characteristics in each bandwidth. The antenna can be applied to GPS, Beidou Satellite Navigation, Bluetooth (2.4–2.485 GHz), WLAN (2.4–2.48 GHz), LTE Band40 (2300–2400 MHz), ISM Band (2.420–2.4835 GHz), WiMAX (2.3 GHz), TD-SCDMA (1880–2025 MHz), WCDMA (1920–2170 MHz), CDMA2000 (1920–2125 MHz), and WLAN (802.11a/*n*: 5.15–5.35 GHz). In future research, on the one hand, it is hoped that the antenna can be combined into an array to increase the gain; on the other hand, it is hoped that the antenna can be designed into a flexible material and applied to a flexible wearable terminal.

Data Availability

The simulation and test data used to support the findings of this study are included within the article.

Conflicts of Interest

The authors declare that they have no conflicts of interest.

Acknowledgments

This work was supported in part by Natural Science Foundation of Hebei Province (no. F2021508009), National Key R&D Project (no. 2020YFC1511805), Fundamental Research Funds for the Central Universities (no. 3142018048), and Education and Teaching Reform Special Project of NCIST (nos. 01010403–55 and 0502010223–16).

References

[1] Z. Yu, J. G. Yu, and X. Y. Ran, "A novel ancient coin-like fractal multiband antenna for wireless applications," *International Journal of Antennas and Propagation*, vol. 2017, Article ID 6459286, 10 pages, 2017.

[2] X. Y. Ran, Z. Yu, and T. Y. Xie, "A novel dual-band binary branch fractal bionic antenna for mobile terminals," *International Journal of Antennas and Propagation*, vol. 2020, Article ID 6109093, 9 pages, 2020.

[3] Z. Yu, Li Yao, Z. Lin, X. Ran, and M. Atsushi, "Design of window grille shape-based multiband Antenna for mobile terminals," *International Journal of Antennas and Propagation*, vol. 2021, Article ID 6684959, 14 pages, 2021.

[4] Z. Yu, Z. Lin, X. Ran et al., "A novel "回" pane structure multiband microstrip antenna for 2G/3G/4G/5G/WLAN/navigation applications," *International Journal of Antennas and Propagation*, vol. 2021, Article ID 5567417, 15 pages, 2021.

[5] P. M. Paul, K. Kandasamy, and M. S. Sharawi, "A triband circularly polarized strip and SRR-Loaded slot antenna," *IEEE Transactions on Antennas and Propagation*, vol. 66, no. 10, pp. 5569–5573, 2018.

[6] S. Ullah, S. Ahmad, B. A. Khan, F. A. Tahir, and J. A. Flint, "An hp-shape hexa-band antenna for multi-standard wireless co mmunication systems," *Springer US*, vol. 25, no. 3, 2019.

[7] T. Dabas, B. K. Kanaujia, D. Gangwar, A. K. Gautam, and K. Rambabu, "Design of multiband multipolarised single feed patch antenna," *IET Microwaves, Antennas & Propagation*, vol. 12, no. 15, pp. 2372–2378, 2018.

[8] Z. Chen, Y. L. Ban, J. H. Chen, J. L. W. Li, and Y. J. Wu, "Bandwidth enhancement of LTE/WWAN printed mobile phone antenna using slotted ground structure," *IEEE Antennas and Wireless Propagation Letters*, vol. 17, no. 8, pp. 1557–1560, 2018.

[9] M. T. Wu and M. L. Chuang, "Multibroadband slotted bow-tie monopole antenna," *IEEE Antennas and Wireless Propagation Letters*, vol. 17, no. 2, pp. 331–334, 2018.

[10] L. Wang, J. Yu, and T. Xie, "The design of a multi-band bionic antenna for mobile terminals," *International Journal of RF and Microwave Computer-Aided Engineering*, vol. 31, no. 6, pp. 1–9, 2021.

[11] M. E. Yassin, H. A. Mohamed, E. A. F. Abdallah, and H. S. El-Hennawy, "Single-fed 4G/5G multiband 2.4/5.5/28 GHz antenna," *IET Microwaves, Antennas & Propagation*, vol. 13, no. 3, pp. 286–290, 2019.

[12] A. Kumar, V. Sankhla, J. Kumar Deegwal, and A. Kumar, "An offset CPW-fed triple-band circularly polarized printed antenna for multiband wireless applications," *AEUE-International Journal of Electronics and Co mmunications*, vol. 86, 2018.

[13] V. Sharma, N. Lakwar, N. Kumar, and T. Garg, "Multiband low-cost fractal antenna based on parasitic split ring resonators," *IET Microwaves, Antennas & Propagation*, vol. 12, no. 6, pp. 913–919, 2018.

[14] T. A. Elwi and A. M. Al-Saegh, "Further realization of a flexible metamaterial based antenna on indium nickel oxide polymerized palm fiber substrates for RF energy harvesting," *International Journal of Microwave and Wireless Technologies*, vol. 5, no. 4, pp. 1–9, 2020.